

Electronic Supplementary Information

Electronegative Guests in CoSb₃

Bo Duan,^{‡ab} Jiong Yang,^{‡ac} James R. Salvador,^d Yang He,^e Bo Zhao,^a Shanyu Wang,^a Ping Wei,^{ab}
Fumio S. Ohuchi,^a Wenqing Zhang,^{*c} Raphaël P. Hermann,^f Olivier Gourdon,^g Scott X. Mao,^e
Yingwen Cheng,^h Chongmin Wang,ⁱ Jun Liu,^h Pengcheng Zhai,^b Xinfeng Tang,^b Qingjie Zhang,^{*b}
and Jihui Yang^{*a}

^aMaterials Science and Engineering Department, University of Washington, Seattle, WA 98195, USA. E-mail:
jihuiy@uw.edu

^bState Key Laboratory of Advanced Technology for Materials Synthesis and Processing, Wuhan University of
Technology, Wuhan 430070, China. E-mail: zhangqj@whut.edu.cn

^cMaterials Genome Institute, Shanghai University, Shanghai 200444, China. E-mail: wqzhang@mail.sic.ac.cn

^dChemical and Materials Systems Lab, General Motors R&D Center, Warren, MI 48090, USA.

^eDepartment of Mechanical Engineering and Materials Science, University of Pittsburgh, Pittsburgh, PA 15261,
USA.

^fMaterials Science and Technology Division, Oak Ridge National Laboratory, Oak Ridge, TN 37831, USA.

^gResearch and Development, ZS Pharma, Coppell, TX 75019, USA.

^hEnergy and Environment Directorate, Pacific Northwest National Laboratory, Richland, WA 99352, USA.

ⁱEnvironmental Molecular Sciences Laboratory, Pacific Northwest National Laboratory, Richland, WA 99352, USA.

[‡] Authors contributed equally.

This file includes:

Figures S1-S12

Tables S1-S3

References 1-10

1. ABF-STEM images of Br-filled sample $\text{Br}_{0.04}\text{Co}_4\text{Sb}_{11.84}$

ABF-STEM observation was used to directly identify the Br-ion in $\text{Br}_{0.04}\text{Co}_4\text{Sb}_{11.84}$ (Fig. S1a-c). EDX data in Fig. S1d shows Br peaks besides Co and Sb. Note that the Cu peaks are originated from the TEM copper grid. Enlarged unit-cell image in Fig. S1b shows clear contrast at guest position (arrow in Fig. S1b) which is consistent with the structure model, providing solid proof of the presence of guest atoms. A line-profile (Fig. S1c) extracted from the ABF signal (reversed for visual convenience) shows the distinct but varying intensity corresponding to the guest positions. The relatively lower intensities of void sites compared with Se-filled system (Fig. 1d) should be ascribed to the small filling fraction of Br ~ 0.04 in CoSb_3 .

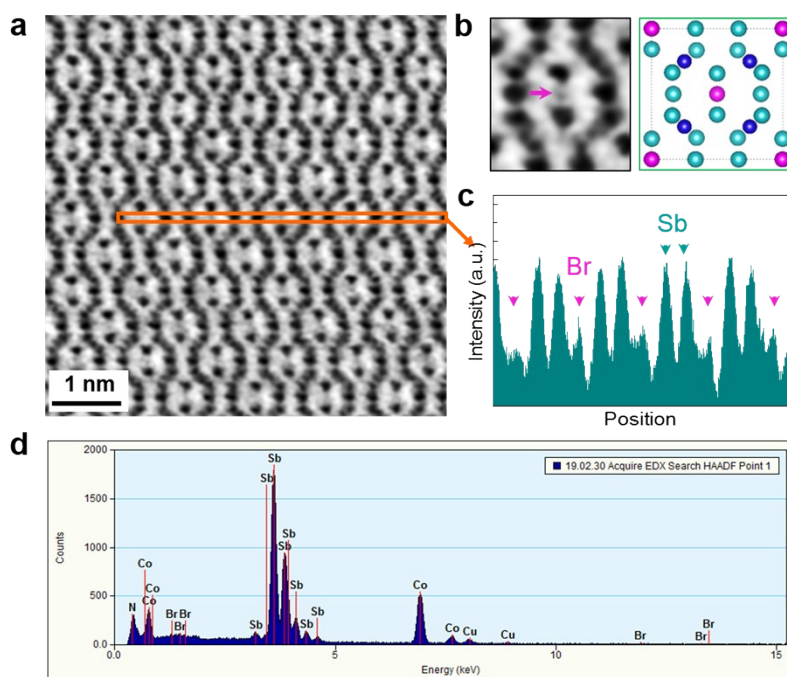


Figure S1 Microstructure of Br-filled sample $\text{Br}_{0.04}\text{Co}_4\text{Sb}_{11.84}$. (a) ABF-STEM image of Br-filled sample taken along the [100] direction. (b) Detailed atomic arrangement, the pink balls represent guest atoms, the dark blue balls represent Co atoms, and the light blue balls represent Sb atoms. (c) An intensity profile along the box marked in (a) to display the intensity variation including the guest only atomic columns, (d) Energy dispersed x-ray (EDX) spectrum of the sample.

2. X-ray and neutron powder diffraction of EN guest filled samples

Rietveld structural refinements were performed on the patterns shown in Fig. S2 using Fullprof. All samples crystallize in the body centered cubic space group $Im-3$. The published crystal structure of $CoSb_3$ was used as a starting model. The lattice parameters were first refined followed by the peak shape and then the general positions of Sb (Wyckoff position $24g$ (0, y, z)). Due to the highly correlated nature of crystallographic site occupancy and their atomic respective displacement parameters (ADPs) the occupancy of the $2a$ site (0, 0, 0) was first set at a value equal to the nominal composition. Sb and Te have very similar x-ray scattering factors and therefore the $24g$ site for the charge compensated samples was modeled as being fully occupied by Sb, and the $8c$ site was modeled as fully occupied by Co. After refining the lattice, peak shape and $24g$ special positions, the ADPs for each atom were then refined. Finally the ADP of the filler was held constant and then the $2a$ site occupancy was refined. The ADPs of the framework atoms and the filler occupancy were iteratively refined, such that the filler occupancy and ADP were held constant in alternating refinement rounds until all ADPs were positive definite. Table S1 and S2 list the structural parameters and Rietveld refinement details for the all structurally characterized samples. Fig. S3 shows the observed, calculated powder x-ray diffractions patterns as well as the difference from Rietveld refinement. All refinements had a minimum reflection to refinement parameter ratio of at least 29:1.

The results of the refinement of the neutron powder diffraction data are summarized in Table S3. The data, refinements, and difference plots are reported in Fig. S4. The refinement were carried out considering isotropic atomic displacement parameters. The mixed occupation of the $24g$ position by antimony and tellurium could not be resolved due to the small scattering neutron diffraction contrast between these elements (scattering length: $b_c^{Sb} = 5.57$ and $b_c^{Te} = 5.68$ fm),

marginally larger than for x-rays. The refinements were thus carried out with only antimony occupying this site and the occupation of the cobalt site was taken as reference and fixed to 1. Further attempts to include anisotropic atomic displacement parameters did not yield significant improvements for the refinements. A further study of possible anharmonic displacements, as were utilized in the description of the off-centering of Eu in EuTiO_3 ¹ for S to the order 4 and 6 of the Gram-Charlier tensor coefficients also did not provide significant improvement. These higher approximation refinements will require currently unavailable single crystalline material.

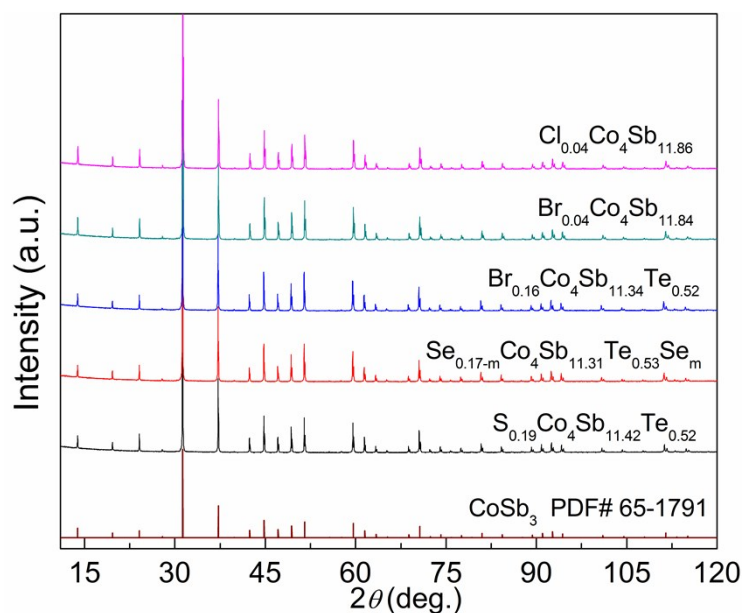


Figure S2 X-ray diffraction of EN guest filled samples. Data were collected over the 2θ ranges 10–120° with a step size of 0.018°. It can be seen that all the samples exhibit single skutterudite phase.

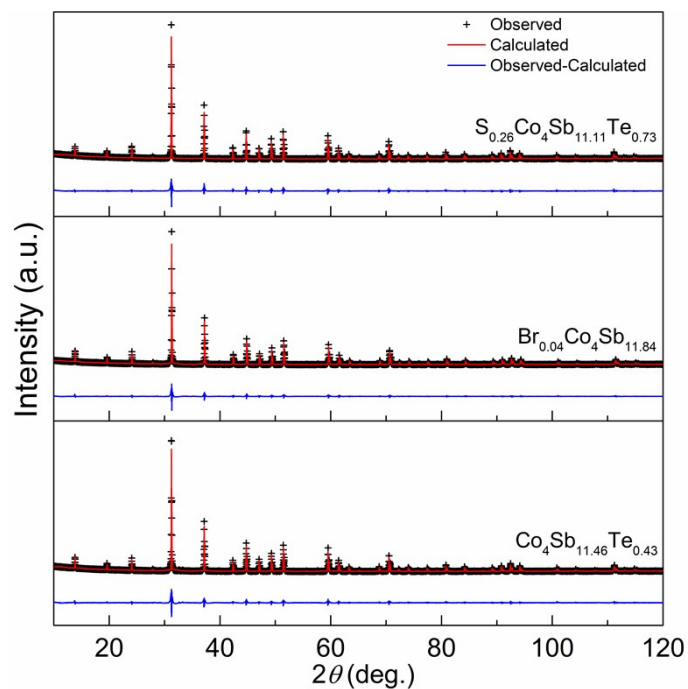


Figure S3 X-ray diffraction refinement. The observed, Rietveld refined, and difference x-ray power pattern intensities for $S_{0.26}Co_4Sb_{11.11}Te_{0.73}$, $Br_{0.04}Co_4Sb_{11.84}$ and $Co_4Sb_{11.46}Te_{0.43}$.

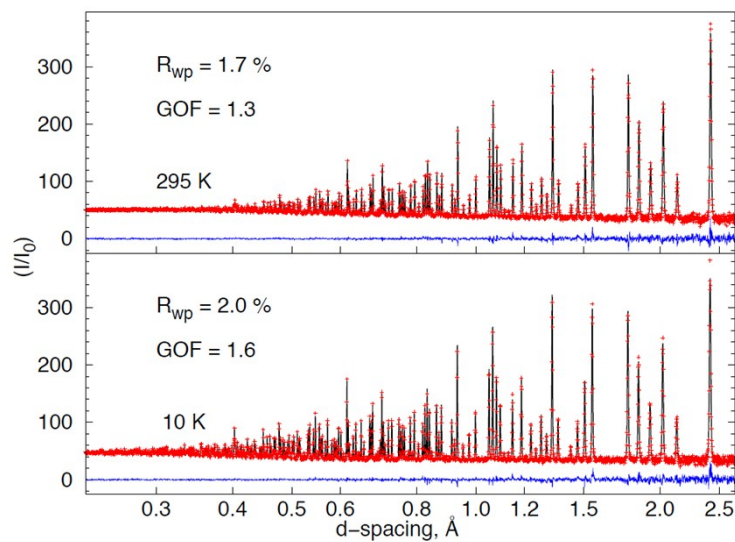


Figure S4 Neutron diffraction refinement. Neutron powder diffraction data (red cross), refinement (black line), and difference (blue line) obtained on 5 g of $S_{0.26}Co_4Sb_{11.11}Te_{0.73}$ at the Powgen, SNS, beam line at 10 K (bottom) and 295 K (top).

Table S1 Summary of Rietveld refinement for charge compensated samples.

EPMA	S_{0.19}Co₄Sb_{11.42}Te_{0.52}	S_{0.26}Co₄Sb_{11.11}Te_{0.73}	Br_{0.16}Co₄Sb_{11.34}Te_{0.52}
<i>a</i> (Å)	9.04825(4)	9.05361(5)	9.05502(4)
Sb <i>y</i>	0.1573(2)	0.1572(2)	0.15746(2)
Sb <i>z</i>	0.3338(2)	0.3338(2)	0.33439(2)
Sb U_{iso} (Å²)	0.0048(5)	0.0012(5)	0.0026(4)
Co U_{iso} (Å²)	0.0015(19)	0.003(2)	0.0012(17)
Filler Occupancy	0.29(3)	0.32(4)	0.240(14)
Filler U_{iso} (Å²)	0.01293	0.05584	0.02275
R_{factor}/%	4.1955	5.2013	4.1154
wR_{factor}/%	6.6036	8.3054	6.5318
χ²/%	6.6132	10.2753	6.7563

Table S2 Summary of Rietveld refinement for uncompensated group Br filled samples, and Te substituted sample, and charge compensated Cl-filled skutterudite.

EPMA	Br_{0.04}Co₄Sb_{11.84}	Cl_{0.18}Co₄Sb_{11.36}Te_{0.51}	Co₄Sb_{11.46}Te_{0.43}
<i>a</i> (Å)	9.03699(4)	9.04965(3)	9.05011(4)
Sb <i>y</i>	0.1575(2)	0.1575(2)	0.1576(2)
Sb <i>z</i>	0.33476(18)	0.33440(19)	0.3346(2)
Sb U_{iso} (Å²)	0.0030(4)	0.0029(4)	0.0041(5)
Co U_{iso} (Å²)	0.0034(18)	0.0017(18)	0.003(2)
Filler Occupancy	0.065(14)	0.38(3)	-
Filler U_{iso} (Å²)	0.04808	0.02619	-
R_{factor}/%	4.4145	4.1370	4.7139
wR_{factor}/%	6.7445	6.6097	7.7633
χ^2/%	7.6103	6.8389	9.6288

Table S3 Summary of neutron powder diffraction refinement for $S_{0.26}Co_4Sb_{11.11}Te_{0.73}$ at 10 and 295 K.

EPMA	$S_{0.26}Co_4Sb_{11.11}Te_{0.73}$	$S_{0.26}Co_4Sb_{11.11}Te_{0.73}$
	10 K	295 K
a (Å)	9.0401(1)	9.0539(1)
Sb y	0.1581(1)	0.1579(1)
Sb z	0.3358(1)	0.3354(1)
Sb U_{iso} (Å²)	0.0020(1)	0.0059(1)
Co U_{iso} (Å²)	0.0017(1)	0.0039(2)
Filler Occupancy	0.27(3)	0.26(3)
Filler U_{iso} (Å²)	0.008(2)	0.008(2)
$R_{factor}/\%$	3.12	2.85
$wR_{factor}/\%$	1.98	1.67
$\chi^2=GOF^2/\%$	2.43	2.02

3. Thermal stability of EN guest filled skutterudites

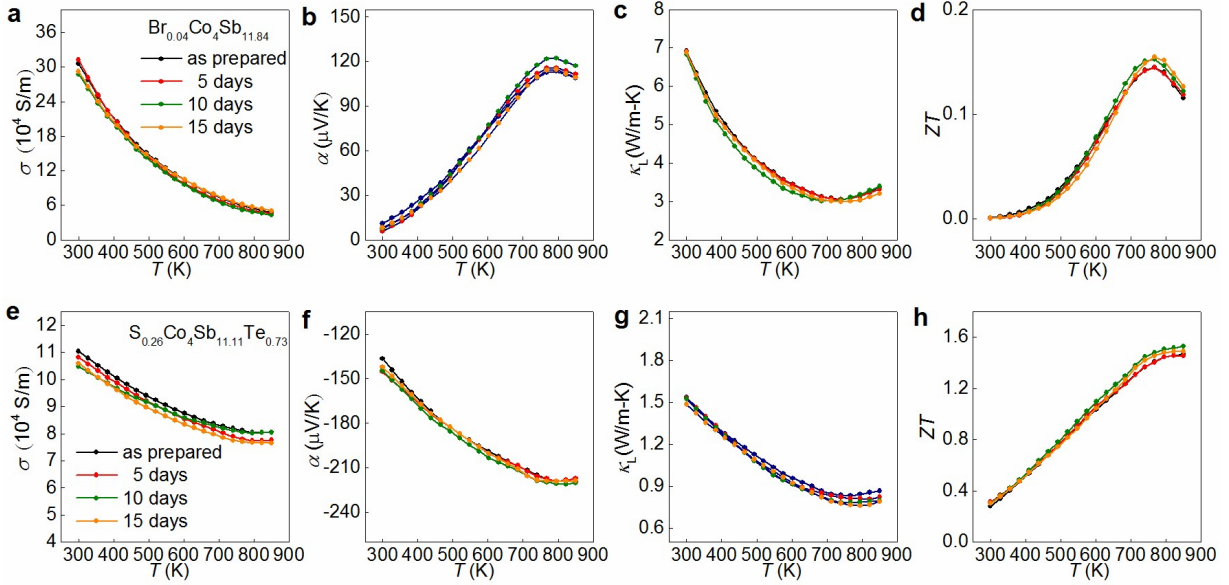


Figure S5 Thermal stability of EN guest filled skutterudites. Temperature dependences of electrical conductivity, Seebeck coefficient, lattice thermal conductivity, and dimensionless figure of merit ZT of the as-prepared $\text{Br}_{0.04}\text{Co}_4\text{Sb}_{11.84}$ (a,b,c,d) and $\text{S}_{0.26}\text{Co}_4\text{Sb}_{11.11}\text{Te}_{0.73}$ (e,f,g,h) and after 5 days, 10 days and 15 days heat treatment. The heat treatment was performed at 873 K in vacuum.

4. Phonon dispersion in CoSb_3 , $\text{Cl}_{0.5}\text{Co}_4\text{Sb}_{11}\text{Te}_1$, and $\text{Yb}_{0.5}\text{Co}_4\text{Sb}_{12}$

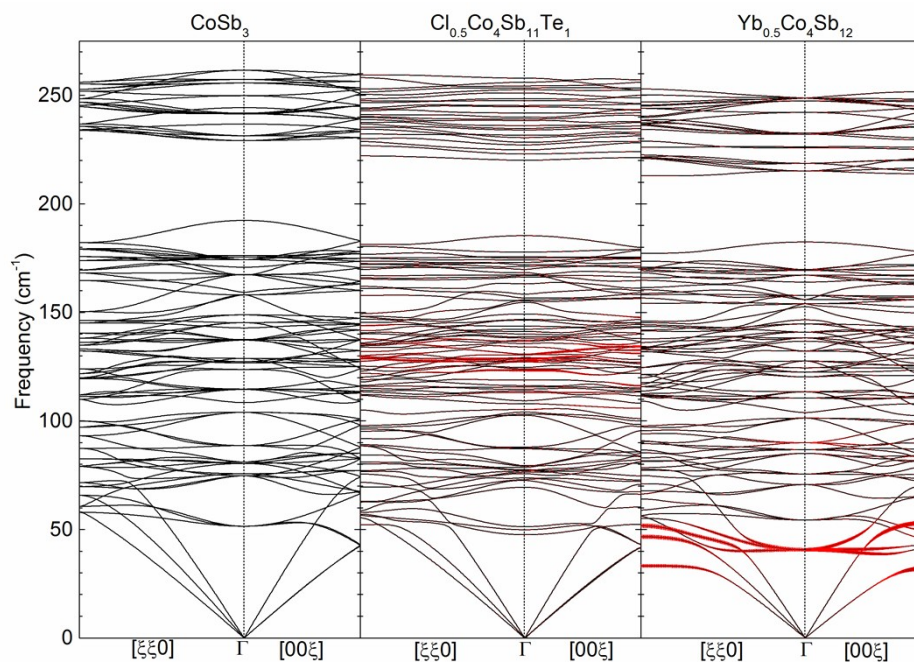


Figure S6 Phonon dispersion in CoSb_3 , $\text{Cl}_{0.5}\text{Co}_4\text{Sb}_{11}\text{Te}_1$ and $\text{Yb}_{0.5}\text{Co}_4\text{Sb}_{12}$. Vertical bars represent the strength of phonon characters from certain atoms.

5. Thermoelectric transport properties of Cl- and Br-filled *p*-type skutterudites.

Cl and Br guests provide holes to the host due to their large electronegativity, and form strong *p*-type filled $R_y\text{Co}_4\text{Sb}_{12}$ (Fig. S7b and Table 1), which are the first discovered *p*-type skutterudites by filling via conventional equilibrium preparation method. Cl- and Br-filled *p*-type samples show similar thermoelectric transport properties. Comparing with pristine $\text{CoSb}_{2.99}$, the room temperature electrical conductivities are greatly enhanced by Cl/Br filling due to the increase of more than one order of magnitude hole concentration (Table 1). Both Cl- and Br-filled samples exhibit rapidly decrease in electrical conductivity with temperature, reflecting metallic behavior. The very low Seebeck coefficient values indicate the hole transport is dominated by the Sb-*p*-bands with light band character,² consistent with the band structure calculations. The lattice thermal conductivity decreases from 8.9 W/m-K for $\text{CoSb}_{2.99}$ to 6.8 W/m-K for $\text{Cl}_{0.04}\text{Co}_4\text{Sb}_{11.86}$ and 6.9 W/m-K for $\text{Br}_{0.04}\text{Co}_4\text{Sb}_{11.84}$ at 300 K. Here Cl and Br only introduce high frequency rattling modes, $\sim 100\text{ cm}^{-1}$ for Br and $\sim 130\text{ cm}^{-1}$ for Cl close to those of alkaline metals (Na $\sim 110\text{ cm}^{-1}$ and K $\sim 140\text{ cm}^{-1}$),³ primarily due to their light weights and large ionic radii. For phonon resonant scattering, only the lattice phonons with frequencies close to the rattling modes of guests could be effectively scattered, and the low frequency acoustic phonons predominantly contribute to the heat conduction in solids.^{4, 5} The high rattling frequencies of Br and Cl in CoSb_3 is the main reason for their limited influence on κ_L reduction, together with their low filling fractions. *ZT* values of Cl- and Br-filled samples were enhanced only at 700-850 K temperature range as compared with $\text{CoSb}_{2.99}$, due to the suppressed bipolar transport at high temperatures.

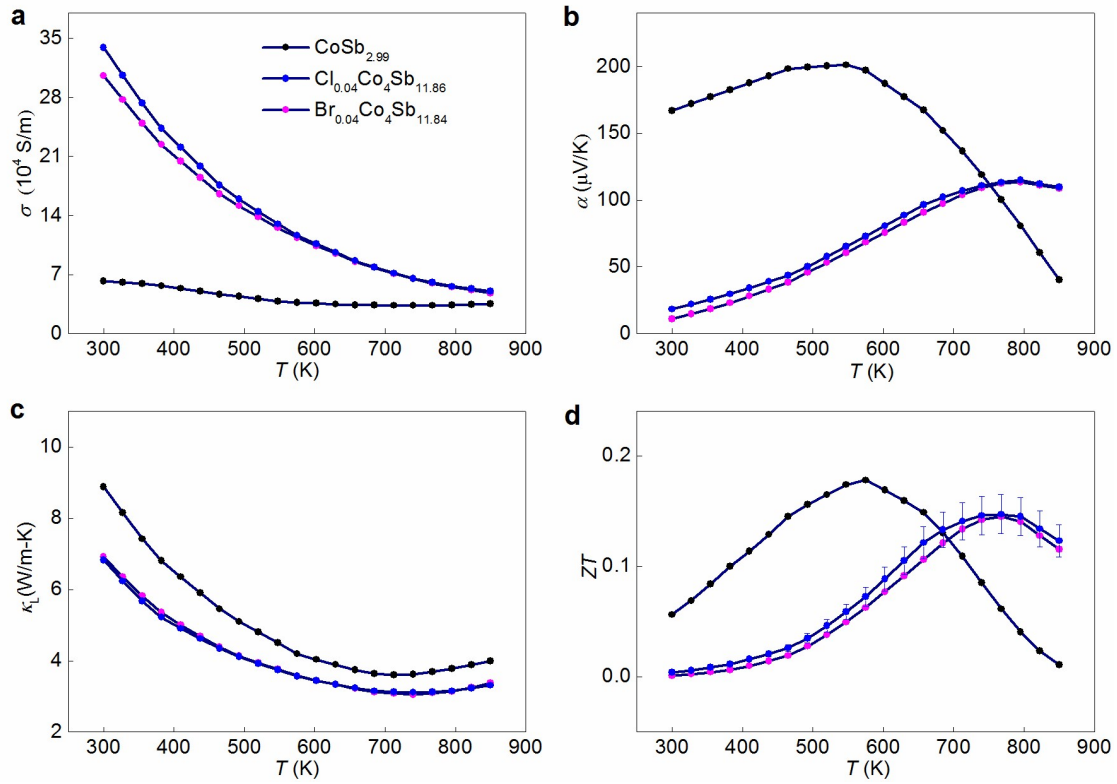


Figure S7 Thermoelectric transport properties of EN guest filled *p*-type skutterudites. Temperature dependence of electrical conductivity (a), Seebeck coefficient (b), lattice thermal conductivity (c), and dimensionless figure of merit ZT (d). The data of pristine $\text{CoSb}_{2.99}$ are also plotted for the sake of comparison.

6. Phonon dispersion in $\text{Rb}_8\text{Al}_6\text{Si}_{40}$ and $\text{Se}_8\text{P}_{16}\text{Si}_{30}$

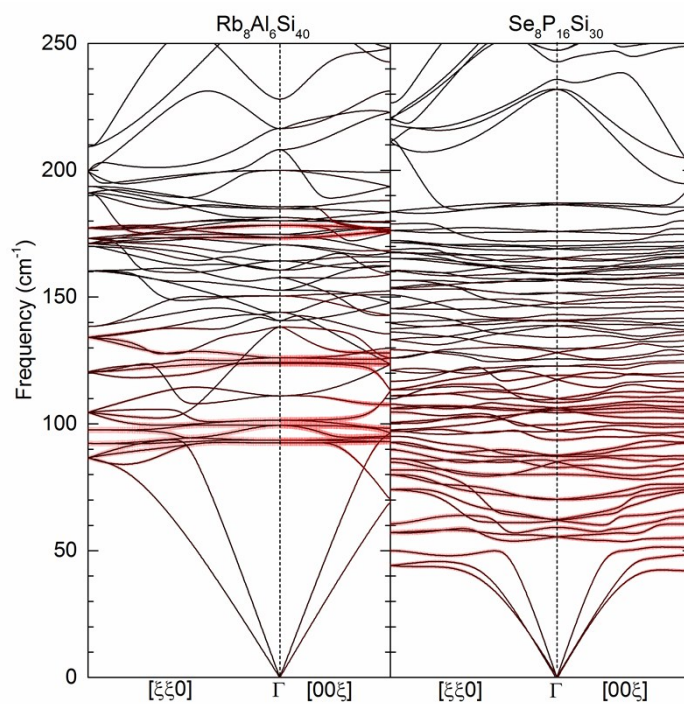


Figure S8 Phonon dispersion in $\text{Rb}_8\text{Al}_6\text{Si}_{40}$ and $\text{Se}_8\text{P}_{16}\text{Si}_{30}$. Vertical bars represent the strength of phonon characters from certain atoms.

7. AIMD simulations of S-filled skutterudite

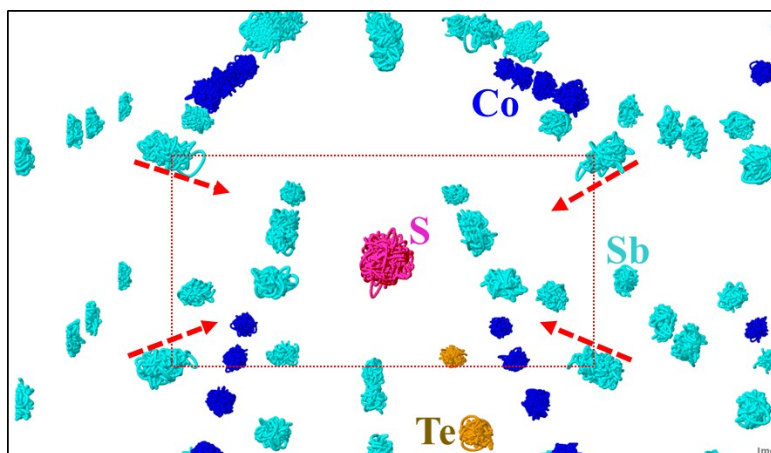


Figure S9 Trajectory of S, Co, Sb and Te atoms of $S_{0.063}Co_4Sb_{11.5}Te_{0.5}$ skutterudite from AIMD simulations. The simulation temperature was set to be 300 K, and the total simulation time was longer than 30 ps.

8. Chemical state of S and Br guests in filled skutterudites

Figure S10a-b show the total and guest-projected DOS for S- and Br-filled skutterudites. The zero energy point corresponds to the Fermi level. In both figures, the projected DOS for the guests are well below their Fermi levels, with the electronic states from Br having a deeper energy window. These results are also supported by our XPS measurements. As shown in Fig. S10c, the binding energy of S $2s$ peak in $S_{0.26}Co_4Sb_{11.11}Te_{0.73}$ is clearly lower than that of the elemental S, indicative of a negative charge on S. A negative charge could also be verified for Br in $Br_{0.04}Co_4Sb_{11.84}$ (Fig. S10d). Damped least-squares fit of Br $3p$ spectra reveals Br $3p_{3/2}$ peak position at ~ 181.8 eV with a spin-orbital splitting of 6.73 eV from Br $3p_{1/2}$ peak. This binding energy is comparable to those of ionic compounds CsBr (181.7 eV) and NaBr (182.1 eV),⁶ where Br is known as Br^{-1} . Thus, it can be predicted that Br is likely to be negatively charged as well in Br-filled samples.

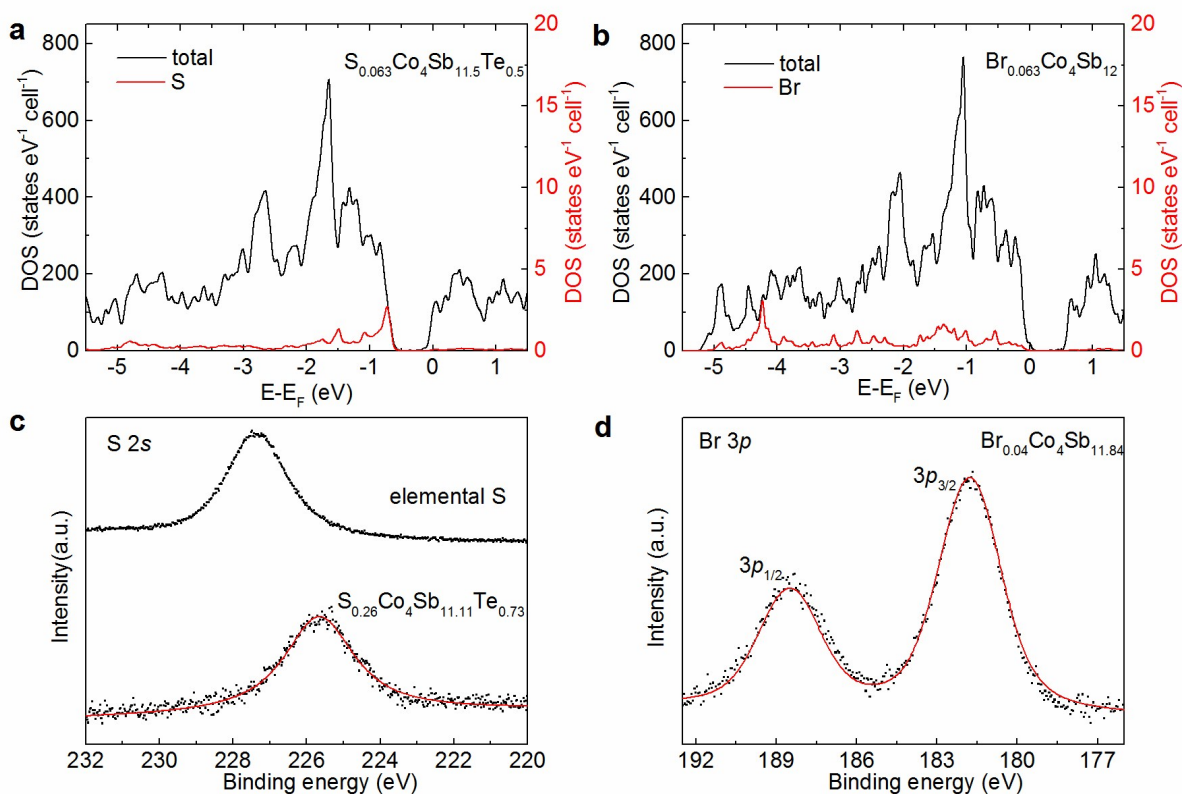


Figure S10 Chemical state of S and Br guest in filled skutterudites. (a,b) Total and projected (on guests) density of states (DOS) for $Br_{0.063}Co_4Sb_{12}$ (a) and $S_{0.063}Co_4Sb_{11.5}Te_{0.5}$ (b). The Fermi level is at the zero energy point. (c,d) XPS spectra of Br 3p (c) and S 2s (d) core levels for $Br_{0.04}Co_4Sb_{11.84}$ and $S_{0.26}Co_4Sb_{11.11}Te_{0.73}$. The data of elemental S 2s core levels are plotted for comparison with that of S-filled sample in (c). All XPS high resolution scans were taken with 23.5 eV passing energy and step size of 0.025 eV.

9. Seebeck coefficient and carrier mobility as functions of carrier concentration of *n*-type EN guest filled skutterudites

As shown in Fig. S11a, EN guest filled $R_y\text{Co}_4\text{Sb}_{12-z}\text{Te}_z$ in this study exhibit the similar α - n_H trend to the Pd- or Te-doped skutterudites⁷ and also comparable to the traditional EP guest filled $R_y\text{Co}_4\text{Sb}_{12}$ ⁸ in the range of electron concentrations investigated here. According to the Pisarenko lines, the effective mass (m^*) of EN guest filled $R_y\text{Co}_4\text{Sb}_{12-z}\text{Te}_z$ increases with increasing electron concentration, consistent with the band nonparabolicity. Similar to the traditional EP guest filled $R_y\text{Co}_4\text{Sb}_{12}$,^{8,9} in which guests solely adjust the carrier concentration and exert negligible influence on band detail (rigid band approximation), the EN-guests in skutterudites in this study also show similar behavior. Fig. S11b shows the mobility vs. concentration. Data from this study and the literatures^{7, 10} (EP guest filled skutterudites and Pd- or Te-doped skutterudites) are compared. The μ_n - n_H data of EN guest filled $R_y\text{Co}_4\text{Sb}_{12-z}\text{Te}_z$ agree well with the trend of Pd- or Te-doped samples, indicating that the EN guests have negligible influence on the electron transport in skutterudites, analogue to the EP guests.¹⁰ Due to the strong ionized impurity scattering by Te ions, the mobilities of EN guest filled $R_y\text{Co}_4\text{Sb}_{12-z}\text{Te}_z$ are much lower as compared with those of EP guest filled $R_y\text{Co}_4\text{Sb}_{12}$ at a given concentration. The mobility is ~ 55 - 35 $\text{cm}^2/\text{V}\cdot\text{s}$ for EP guest filled samples, while only ~ 30 - 20 $\text{cm}^2/\text{V}\cdot\text{s}$ for EN guest filled Te-doped samples at the electron concentration range of 2 - 6×10^{20} cm^{-3} .

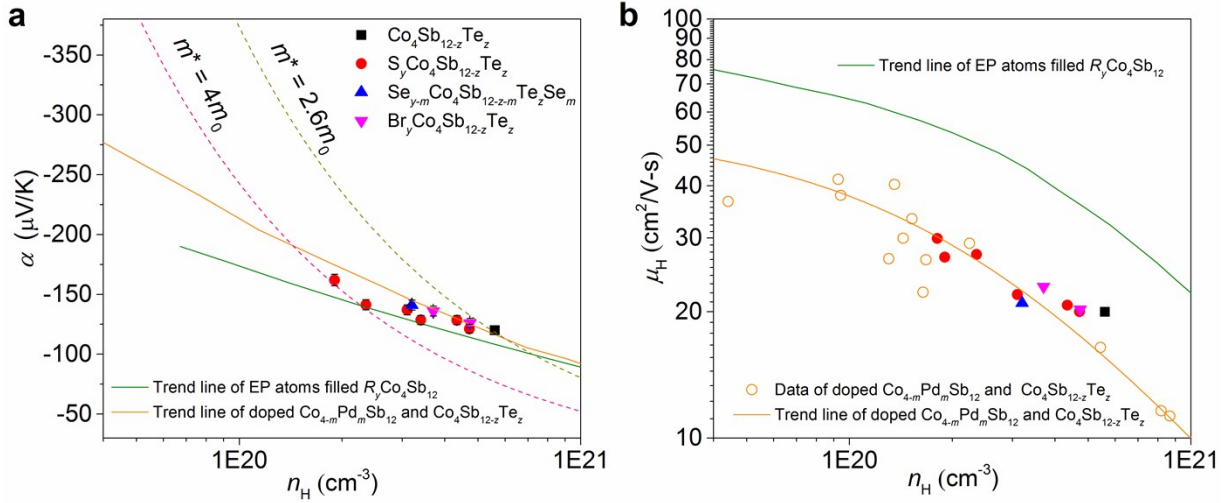


Figure S11 Seebeck coefficient and carrier mobility as functions of carrier concentration of *n*-type EN guest filled skutterudites. (a) The room temperature Seebeck coefficient as a function of carrier concentration for EN guest filled Te-doped skutterudites. The green solid line is the trend for EP guest filled $R_y\text{Co}_4\text{Sb}_{12}$,⁸ and the orange solid line is the trend for Pd or Te doped samples.⁷ The pink and dark yellow dashed lines are the Pisarenko lines of $m^* = 2.6m_0$ and $4m_0$, respectively. (b) The room temperature carrier mobility as a function of carrier concentration for EN guest filled Te-doped skutterudites. The orange circles are the data of Pd- or Te- doped skutterudites.⁷ The green solid line is the trend for EP guest filled $R_y\text{Co}_4\text{Sb}_{12}$,¹⁰ and the orange solid line is the trend for Pd- or Te-doped samples.

10. Specific heat used for thermal conductivity calculation

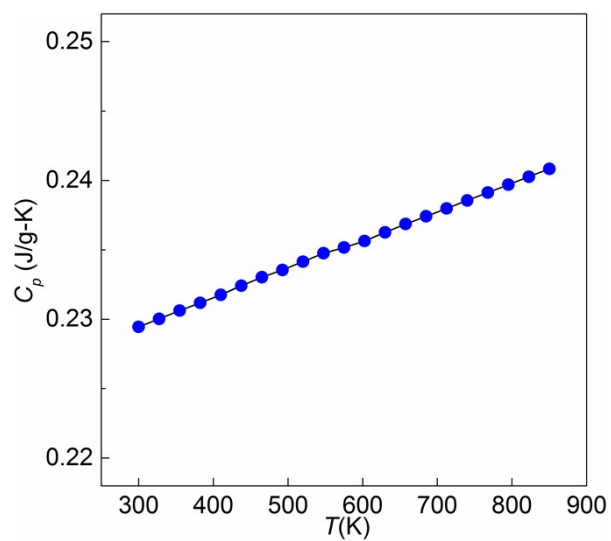


Figure S12 Temperature dependence of specific heat (C_p) used in this work in the range of 300-850 K.

References

1. D. Bessas, K. Z. Rushchanskii, M. Kachlik, S. Disch, O. Gourdon, J. Bednarcik, K. Maca, I. Sergueev, S. Kamba, M. Lezaic and R. P. Hermann, *Phys. Rev. B*, 2013, **88**, 144308.
2. D. J. Singh and W. E. Pickett, *Phys. Rev. B*, 1994, **50**, 11235-11238.
3. J. Yang, W. Zhang, S. Q. Bai, Z. Mei and L. D. Chen, *Appl. Phys. Lett.*, 2007, **90**, 192111.
4. X. Shi, S. Q. Bai, L. L. Xi, J. Yang, W. Q. Zhang, L. D. Chen and J. H. Yang, *J. Mater. Res.*, 2011, **26**, 1745-1754.
5. Z. T. Tian, S. Lee and G. Chen, *J. Heat Transfer* 2013, **135**, 061605.
6. J. Sharma and Z. Iqbal, *Chem. Phys. Lett.*, 1978, **56**, 373-376.
7. T. Caillat, A. Borshchevsky and J.-P. Fleurial, *J. Appl. Phys.*, 1996, **80**, 4442-4449.
8. S. Q. Bai, Y. Z. Pei, L. D. Chen, W. Q. Zhang, X. Y. Zhao and J. Yang, *Acta Mater.*, 2009, **57**, 3135-3139.
9. V. L. Kuznetsov, L. A. Kuznetsova and D. M. Rowe, *J. Phys.: Condens. Matter*, 2003, **15**, 5035-5048.
10. X. Shi, J. Yang, J. R. Salvador, M. F. Chi, J. Y. Cho, H. Wang, S. Q. Bai, J. H. Yang, W. Q. Zhang and L. D. Chen, *J. Am. Chem. Soc.*, 2011, **133**, 7837-7846.